2014 Canada-China Conference on Advanced Reactor Development (CCCARD-2014)
Niagara Falls Marriott Fallsview Hotel & Spa, Niagara Falls, Ontario Canada, April 27-30, 2014.

CCCARD2014-xxx

# MEASUREMENTS OF THE EFFECTS OF A WIRE-WRAP SPACER ON THE THERMALHYDRAULICS OF HEATED ANNULAR UPWARD FLOW OF SUPERCRITICAL R134a IN STEADY AND TRANSIENT CONDITIONS

**S. Reinink, A. Copping, S. Kedare, K. Hovell, M. I. Yaras**
Carleton University, Ottawa, Canada
metin.yaras@carleton.ca

## Abstract

Experiments were conducted at supercritical pressures and temperatures on a vertically-oriented annular heating rod with a wire-wrap spacer using upward-flowing R134a to determine the effect of a wire-wrap spacer on heat transfer in proximity of the pseudocritical point. Measurements were taken at quasi-steady-state and pressure-transient conditions. During each instance of deteriorated heat transfer, the Nusselt number is greater than values predicted by the Dittus-Boelter correlation. Heat transfer during the pressure transients is observed to be insensitive to the time rate of change of the fluid pressure, which implies that the transience does not affect the instantaneous state of the heat-transfer process.

## 1. Introduction

The Supercritical Water-Cooled Reactor (SCWR) concept is considered as the next step in the development of nuclear reactors. The SCWR will use water at a supercritical thermodynamic state to increase the power cycle maximum temperature which will significantly improve the thermal efficiency. In addition, the lack of phase change implies a simpler, more compact design. The SCWR will operate frequently in the trans-pseudocritical regime, in which the working fluid experiences significant changes in thermophysical properties for small changes in temperature and pressure. It has been observed that empirical correlations for predicting the convective heat transfer coefficient at subcritical temperatures cannot accurately predict convective heat transfer at temperatures near the pseudocritical point. Heat transfer rates which are higher and lower than those predicted by correlations for subcritical temperatures are referred to as improved heat transfer (IHT) and deteriorated heat transfer (DHT), respectively [1].

Numerous experimental studies have observed and documented the trends of IHT and DHT near the pseudocritical point for flows in heated tubular geometries (*e.g.*, [1], [2]). Only a few studies in literature have investigated heat transfer near the pseudocritical point for geometries other than tubular, or geometries with a wire-wrap spacer in either an annular or bundle configuration. Licht et al. [3] used a supercritical water facility to investigate heat transfer in a square annular flow channel and compared their results to available correlations for predicting heat transfer around the critical point. Li et al. [4] and Wang et al. [5] experimentally studied the effect of a helically-wrapped wire and a spiral spacer in a square and a circular vertical

channel, respectively; they found that the wrapped wire partially eliminated heat transfer deterioration. Studies on heat transfer around the critical point are also largely restricted to steady state conditions. Kang and Chang [6] were the first to quantitatively study heat transfer characteristics in transient conditions. They assessed the applicability of steady-state heat transfer correlations to conditions during pressure transients, and discovered that varying the pressure transient rate had a trivial effect on the heat transfer rate.

The goal of the present study is to further shed light on the effects of a wire-wrap spacer in an annular configuration on heat transfer around the critical point at steady state and transient conditions. Since the critical pressure and temperature of water ($P_c$ = 22.064 MPa and $T_c$ = 647.1 K, respectively) yield a challenging environment for conducting experimental measurements, measurements are taken using R134a as the working fluid, in which the critical point occurs at 4.06 MPa and 100.9°C. Figure 1 presents the distribution of selected thermophysical properties near the critical point for R134a.

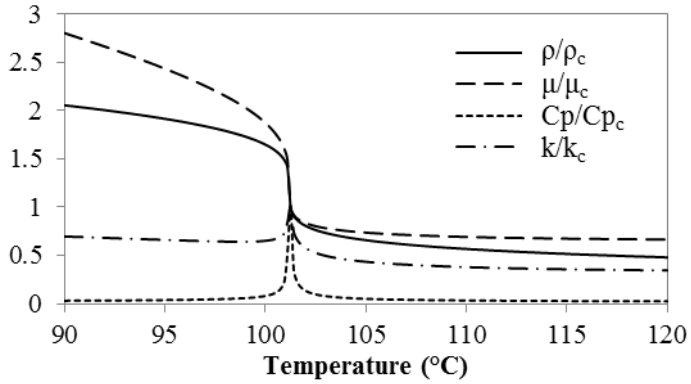


Figure 1 Variation of selected thermophysical properties of R134a at the critical pressure (subscript "c" denotes the value at the critical point)

## 2. Experimental facility

The heated annulus flow experiments were performed on the Carleton R134a test loop (CR134a Loop). Figure 2 illustrates the primary components of the loop. An electrical feed system provides the facility with electric power for joule heating of the working fluid in the test section. The heat absorbed by the working fluid is then transferred to a water-glycol mixture via a shell-plate heat exchanger, and is then rejected to the atmosphere via a cooling tower. A bladder-type accumulator with control and pressure relief valves is utilized to enable controlled pressurization of the loop and damp any undesirable pressure oscillations that may develop during operation of the loop.

### 2.1 Test-section geometry

The annular test section geometry is shown in Figure 3a and 3b. The test section is installed on the loop in a vertical orientation, with the fluid moving upwards. The wire-wrap spacer is installed with a pitch of 100 mm (10 times the heater rod diameter). This value was selected based on a previous investigation which showed that reducing the pitch from 200 mm to

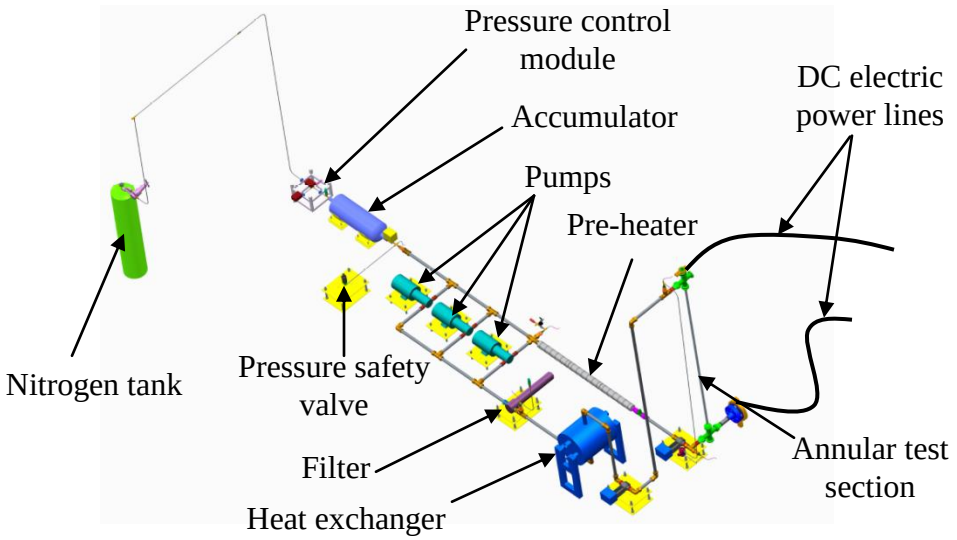


Figure 2 Schematic of the CR134a Loop showing primary components

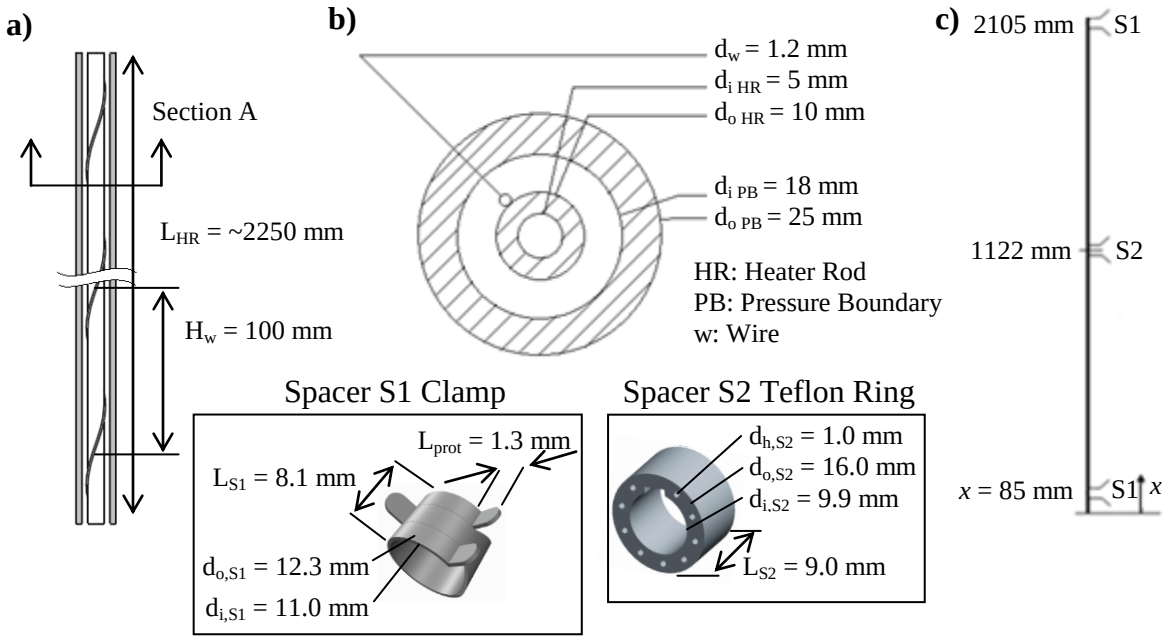


Figure 3 Test-section layout and primary dimensions

100 mm produces a noticeable improvement in convective heat transfer and only a slight increase in the friction factor [7]. In addition to the wire-wrap spacer, "discrete" spacers were installed at several locations along the length of the test section to center the heater rod within the tubular pressure boundary, electrically isolate the heater rod from the pressure boundary, and secure the wire wrap onto the heater rod. Two different discrete spacer types were used. The first spacer type, designated Spacer S1, contains a pair of small clamps installed 7 mm apart in a circumferential orientation to allow for balanced radial support of the heater rod. The second spacer type, designated Spacer S2, consists of a Teflon ring installed on the heater rod between the two clamps used in Spacer S1. The flow is able to pass between the test section pressure boundary and the outer surface of the Teflon ring, as well as through 9 holes

evenly spaced circumferentially on the front face of the spacer. One of the clamps used in Spacer S1 and the Teflon ring used in Spacer S2 are shown as insets in Figure 3. Figure 3c shows the axial locations of the discrete spacers. As discussed in more detail in Section 3.3, heater rod internal temperature measurements were used to verify that significant axial regions were present in which heat transfer rates were not affected by the discrete spacers.

## 2.2 Instrumentation and data acquisition

Table 1 summarizes the primary measurement locations and sensor types on the loop for the present experiments. Secondary sensors for cross-checking the readings of the primary sensors and for operation control and health monitoring include absolute pressure on the nitrogen-filled pressure-control module, a turbine flow meter, DC current and voltage output from the AC/DC transformer, and N-type thermocouples placed at strategic locations along the loop.

Table 1 Summary of primary measurement instrumentation

| *Parameter* | *Instrument* | *Nominal value* | *Uncertainty* |
|---|---|---|---|
| Absolute pressure | Absolute pressure transducer | 4.3 MPa | ± 0.50 % |
| Pressure drop | Differential pressure transducer | ± 40 kPa | ± 1.02 % |
| Mass flux | Ultrasonic flow meter | 580 kg/s/m$^2$ | ± 1.69 % |
| Heater rod internal temperature | K-type thermocouple | n/a | ± 1.78°C |
| Inlet and outlet bulk temperature | N-type thermocouple | n/a | ± 1.23°C |
| Heat flux | Inlet and outlet bulk enthalpies[1] | 105 kW/m$^2$ | ± 1.95 % |
| Nu | Evaluation | 275 | ± 3.84 % |

[1]Bulk enthalpies are determined from pressure and temperature measurements

The K-type thermocouple used to measure heater-rod internal temperature is traversed along the centerline of the heater rod with a stepper-motor-driven pulley system installed above the test section. The thermocouple leads exit the heater rod at its top end which is open to the atmosphere, and are then spooled onto a pulley. This system enables motorized axial positioning of the thermocouple with an accuracy of ±0.22% of the total traversed length (this corresponds to an accumulated positional error of ±5 mm at the end of a traverse from the inlet to the outlet of the test section). To verify that significant regions were present in which heat transfer rates were not affected by the discrete spacers, the K-type thermocouple was traversed from the inlet to the outlet of the test section in 25 mm increments. The long-term average value of the steady signal at each point was established by averaging the signal acquired at a sampling rate of 2 Hz over a 30 second period. For steady-state and transient tests in the supercritical thermophysical state, the K-type thermocouple was maintained at a fixed axial position of x/L = 0.8 (x = 1800 mm) to allow for local wall temperature measurements in time during transient conditions. The axial position was chosen such that the thermocouple was placed near the end of the heater rod where temperatures are highest and heat transfer near the critical thermophysical state will occur first. Additionally, the selected axial position resides in a region where the flow is unaffected by the wake of nearby discrete spacers. Two Teflon plugs with a sliding fit in the heater rod are installed on the thermocouple

leads such that the sensor is enclosed in a very small volume of air trapped between the two plugs. This arrangement ensures negligible convective motion of air around the sensor which would otherwise interfere with accurate temperature measurements.

## 3. Results and discussion

### 3.1 Test conditions

The purpose of the first test was to observe the Nusselt number distribution at temperatures close to the pseudocritical temperature at steady-state conditions. In this test, the heat flux was incrementally increased in small steps of 1 kW/m$^2$, and the conditions were allowed to reach steady state between each step. Given the convergence to a steady state after each heat-flux increment, this test is referred to as a quasi-steady-state test. As the heat flux was increased, the wall temperature at the measurement location of x/L = 0.8 slowly increased such that it approached and then exceeded the pseudocritical temperature. The conditions of this test are summarized in Table 2. The test was repeated at the same conditions to establish repeatability. The Reynolds number, $Re_{local}$, corresponds to the fluid properties at the measurement location and is based on the hydraulic diameter as the length scale.

Table 2 Test matrix for quasi-steady-state tests

| $P/P_c$ | $G$ ($kg/m^2s$) | $Re_{local}$ | $q_w''_{initial}$ ($kW/m^2$) | $q_w''_{final}$ ($kW/m^2$) | $(q_w''/G)_{initial}$ ($kJ/kg$) | $(q_w''/G)_{final}$ ($kJ/kg$) | $T_{in}$ ($°C$) |
|---|---|---|---|---|---|---|---|
| 1.07 | 565 | 38500 | 108 | 123 | 0.191 | 0.215 | 24.6 |

Quasi-steady-state tests were followed by pressure transient tests, in which the pressure was decreased at a contant rate from a steady state condition above the critical pressure to the critical pressure, and the mass flux and heat flux were held constant. The constant rate for the pressure transient is quantified by determining the slope of the corresponding pressure vs. time curve using a linear curve fit. Pressure transient tests investigating the effects of the rate of the pressure transient on heat transfer around the critical point are shown in Table 3. Pressure transient rates were chosen based on rates typical of a mild loss of coolant accident, which are similar to the pressure transients used by Kang and Chang [6].

Table 3 Test matrix for pressure transient tests investigating the effects of the pressure transient rate on heat transfer near the critical point

| $P/P_{c\ initial}$ | $P/P_{c\ final}$ | $dP/dt$ ($kPa/s$) | $G$ ($kg/m^2s$) | $Re_{local}$ | $q_w''$ ($kW/m^2$) | $q_w''/G$ ($kJ/kg$) | $T_{in}$ ($°C$) |
|---|---|---|---|---|---|---|---|
| 1.18 | 1.02 | -1.6 | 582 | 36500 | 107 | 0.185 | 24.1 |
| 1.23 | 1.09 | -3.0 | 582 | 36200 | 108 | 0.185 | 24.7 |
| 1.25 | 1.01 | -8.5 | 584 | 36600 | 108 | 0.185 | 24.9 |

Table 4 summarizes the pressure transient tests which aim to investigate the influence of heat flux value on the heat transfer process as affected by pressure transients, and tests performed for a range of inlet temperatures are listed in Table 5.

Table 4 Test matrix for pressure transient tests investigating the effects of heat flux values on heat transfer near the critical point

| $P/P_{c\ initial}$ | $P/P_{c\ final}$ | $dP/dt$ (kPa/s) | $G$ ($kg/m^2s$) | $Re_{local}$ | $q_w''$ ($kW/m^2$) | $q_w''/G$ (kJ/kg) | $T_{in}$ (°C) |
|---|---|---|---|---|---|---|---|
| 1.22 | 1.01 | -4.8 | 582 | 36500 | 108 | 0.185 | 24.8 |
| 1.24 | 1.02 | -4.9 | 583 | 38600 | 119 | 0.202 | 25.3 |
| 1.25 | 1.02 | -4.8 | 579 | 40200 | 127 | 0.220 | 25.5 |

Table 5 Test matrix for pressure transient tests investigating the effects of inlet temperature on heat transfer near the critical point

| $P/P_{c\ initial}$ | $P/P_{c\ final}$ | $dP/dt$ (kPa/s) | $G$ ($kg/m^2s$) | $Re_{local}$ | $q_w''$ ($kW/m^2$) | $q_w''/G$ (kJ/kg) | $T_{in}$ (°C) |
|---|---|---|---|---|---|---|---|
| 1.24 | 1.03 | -3.4 | 583 | 40500 | 98 | 0.167 | 37.6 |
| 1.24 | 1.02 | -1.9 | 600 | 38900 | 89 | 0.148 | 36.1 |
| 1.22 | 1.02 | -2.1 | 549 | 41800 | 86 | 0.156 | 46.6 |

### 3.2 Data reduction

To assist in the interpretation of the measured heat transfer characteristics, the data was post-processed to yield the local Nusselt number, *Nu*, at the measurement location. The initial steps for evaluating *Nu*, as adapted from [6], are presented in Eqn. (1) and (2), and involve the evaluation of the heater rod outer wall temperature, $T_{wall}$:

$$T_{wall} = T_{i,x} + \frac{\dot{q}_v}{4k_w}\left[\left(\frac{D_{o,HR}}{2}\right)^2 - \left(\frac{D_{i,HR}}{2}\right)^2\right] - \frac{\dot{q}_v}{2k_w}\left(\frac{D_{o,HR}}{2}\right)^2 \ln\frac{D_{o,HR}}{D_{i,HR}} \quad (1)$$

$$\dot{q}_v = \dot{Q}\Big/\left[\frac{\pi}{4}\left(D_{o,HR}^2 - D_{i,HR}^2\right)L_H\right] \quad (2)$$

where $\dot{Q}$ is the heating power generated in the walls of the heater rod, $\dot{q}_v$ is the heating power per unit volume, $T_{i,x}$ is the heater rod inner wall temperature measured by the thermocouple, and $k_w$ is the conductive heat transfer coefficient of the heater rod.

As the heat flux is generated uniformly along the length of the test section, the bulk specific enthalpy of the working fluid (R134a) varies linearly as per the following relationship:

$$H_{b,x} = H_{b,in} + \frac{\dot{Q}}{\dot{m}}\frac{x}{L_H} \quad (3)$$

where $H_{b,in}$ is the specific enthalpy at the test section inlet pressure and temperature, $x$ is the location along the test section, and $\dot{m}$ is the mass flow rate. The local fluid bulk temperature, $T_{b,x}$, can then be determined based on the local specific bulk enthalpy, $H_{b,x}$, and fluid pressure. With the values of $T_{wall,x}$ and $T_{b,x}$ established, and the wall heat flux ($q_w''$) determined from the value of heating power, $\dot{Q}$, the value of the local convective heat transfer coefficient, $h_x$, can be determined using Newton's Law of Convective Cooling:

$$h_x = \frac{q_w''}{(T_{wall,x} - T_{b,x})} \quad (4)$$

### 3.3 Effects of discrete spacers on convection heat transfer along the heater rod

Measurements at supercritical conditions were preceded by preliminary measurements at subcritical temperatures of the axial internal temperature distribution along the heater rod to determine the size of streamwise regions affected by the discrete spacers. In the first test, four S1 spacers were placed at four axial locations along the heater rod to determine the effect of the S1 spacers on heat transfer at different axial locations along the heater rod. In the second test, the first test was repeated with S2 spacers installed at the same respective locations. Measurements were taken at a Reynolds number of 48000 and a pressure of $P/P_c = 1.06$. The results are presented in Figure 4. The locations of the discrete spacers are shown with black-coloured bars near the abscissa.

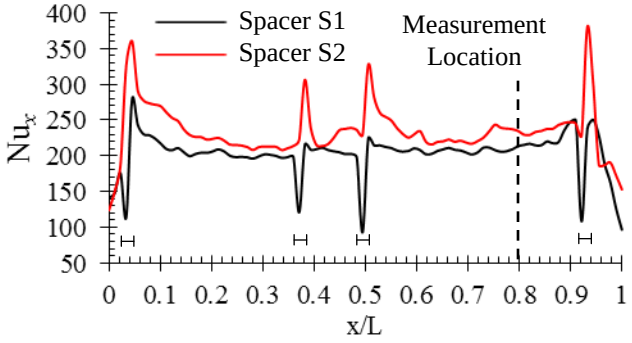


Figure 4 Effect of discrete spacers on heat transfer

The results show that the wake beyond the S1 and S2 spacers does not affect the flow beyond $\Delta x/L \approx 0.15$ downstream of the spacer. Hence, all heater rod temperature measurements during subsequent supercritical tests were taken at a position which is 30% L downstream of the nearest spacer.

### 3.4 Supercritical-fluid tests at steady-state and transient conditions

The results of the quasi-steady-state heat transfer test near the pseudocritical point are shown in Figure 5 through temporal variation of the Nusselt number at $x/L = 0.8$. The test was carried out twice to determine repeatability, with very similar results obtained in each case (only one case is shown in Figure 5). As the wall temperature approaches the pseudocritical point during the first half of the test, the Nusselt number is more than three times greater than the value predicted by the Dittus-Boelter correlation for an annular flow without a wire-wrap spacer. When the wall temperature reaches the pseudocritical temperature, the Nusselt number drops significantly and at a very high rate, indicating deterioration in heat transfer. A recent experimental study with the present test setup at subcritical temperatures showed that the wire-wrap spacer of the present study provides 27% improvement in heat transfer at Reynolds numbers similar to the present tests [7]. Accordingly, the very large differences between the present measurements and the predictions based on the Dittus-Boelter correlation are dominantly caused by physical mechanisms other than the effects of the wire-wrap spacer.

Two to three times increase in heat transfer rates has been regularly observed when the wall temperature is near the pseudocritical temperature (*e.g.*, [1], [2]). Azih and Yaras [8]

performed a direct numerical simulation (DNS) of forced-convection heat transfer in a channel with supercritical water to show that the increase in heat transfer due to changes in turbulent mixing promoted by high property gradients near the pseudocritical temperature is an order of magnitude greater than the heat-transfer increase that can be attributed to changes in molecular thermal diffusion. Based on a DNS of a flat-plate turbulent boundary layer over a heated wall using supercritical water, Azih et al. [9] observed that the wall-normal density and viscosity gradients destabilize the flow resulting in increased concentration of coherent turbulent structures in the near-wall region of the boundary layer. Based on these observations, the improved heat transfer rate in the present data corresponding to wall temperatures less than the pseudocritical temperature is explained by the enhancement of the turbulent mixing mechanism driven by the wall-normal gradients in density and viscosity.

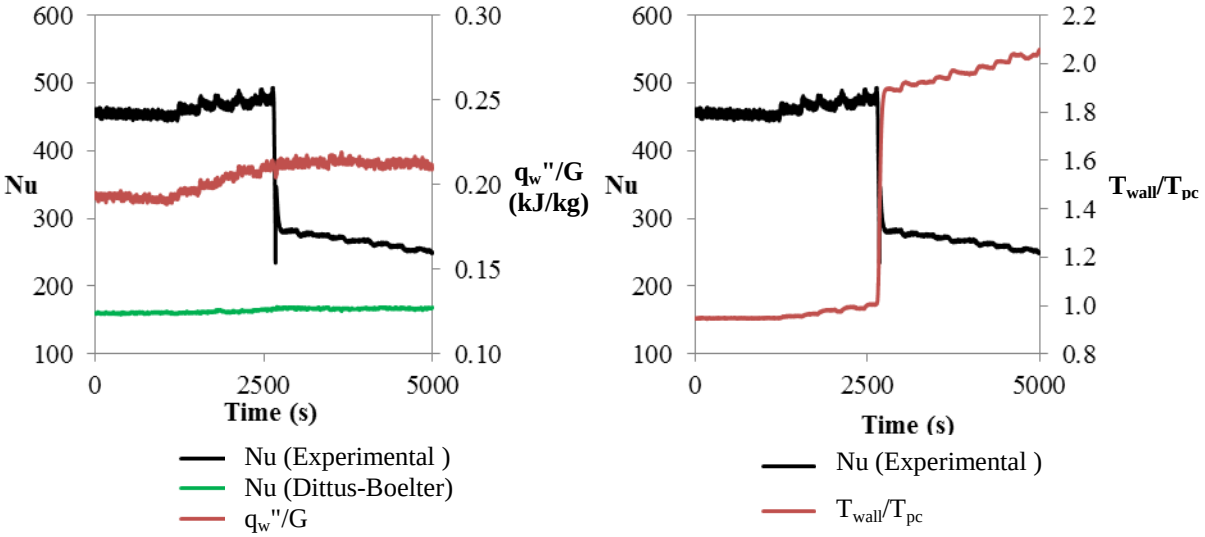


Figure 5 Nusselt number trends in quasi-steady-state tests

The rapid drop in the Nusselt number when the wall temperature reaches the pseudocritical temperature indicates the occurrence of deteriorated heat transfer. Despite the deterioration in heat transfer, the Nusselt number is still significantly greater than values predicted by the Dittus-Boelter correlation for an annular flow with no wire-wrap spacer. This is attributed to the enhanced turbulent mixing promoted by the wire-wrap spacer. Since deteriorated heat transfer is largely due to a reduction in the concentration of coherent turbulent structures in the boundary layer near the wall prompted by the wall-normal density and viscosity gradients [8], it is plausible that enhanced turbulent mixing produced by the presence of the wire-wrap spacer partially offsets the reduction in turbulence driven by the wall-normal density and viscosity gradients. The Nusselt number in the deteriorated heat transfer regime is ~70% higher than the value predicted by the Dittus-Boelter correlation. This is suggestive of enhanced effectiveness of the wire wrap in promoting turbulence when substantial wall-normal gradients exist in thermodynamic properties. This complex interplay between wire-wrap generated turbulence and alteration of coherent structures of turbulence by wall-normal property gradients remains to be understood.

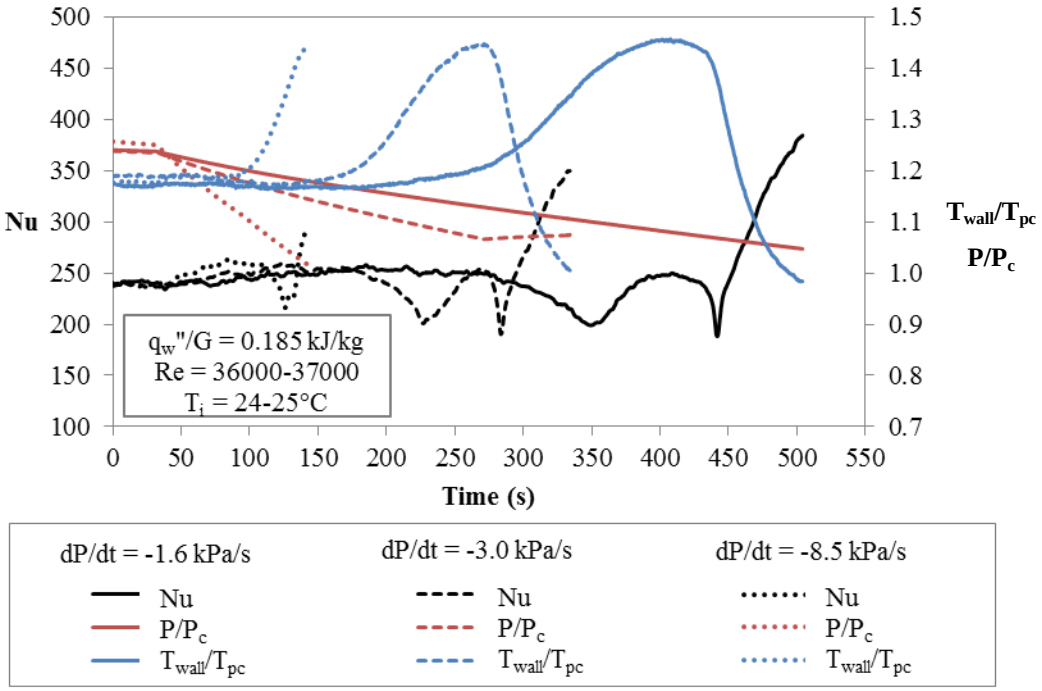


Figure 6 Effect of pressure transient rate on heat transfer during pressure transients

Figure 6 shows the time variation of the Nusselt number, pressure, and wall temperature for several values of temporal gradients in pressure during pressure transients. At each instance in time, the value of pseudocritical temperature, $T_{pc}$, used to normalize the wall temperature, $T_{wall}$, corresponds to the instantaneous value of the fluid pressure. At the beginning of each transient, the wall temperature is above the pseudocritical temperature, and the pressure is equal to about $P/P_c = 1.2$. As the pressure decreases at a constant rate during the transient, the fluid temperature remains relatively constant initially. Accordingly, the density is expected to decrease. Since the fluid temperature near the wall is closer to the critical point, the density decreases by a larger amount for the fluid near the wall than farther away from the wall. As a result, the local mass flux near the wall is reduced, which increases the thermal resistance in the streamwise direction near the wall, prompting the wall temperature to increase. In turn, the increase in wall temperature decreases the local thermal conductivity of the fluid, thus further contributing to the local increase in thermal resistance. The reduction in thermal conduction exceeds that in thermal convection, resulting in about 20% decrease in the value of the Nusselt number. As pressure continues to decrease towards the critical value, the increasing magnitudes of the wall-normal density and viscosity gradients promotes near-wall turbulence, thus reversing the trend in the Nusselt number. As expected, the rapid increase in convection heat transfer yields a reduction in the wall temperature. For the first two cases, the temporal variation in the Nusselt number and wall temperature is dependent on the instantaneous temperature and pressure only, and not on the pressure transient rate. For the highest pressure transient rate, the initiation of improved heat transfer is not able to fully develop due to the thermal inertia of the fluid near the wall.

Sensitivity of the effect of pressure transients on heat transfer to the value of heat flux is illustrated in Figure 7. The Nusselt number during the steady-state period before the pressure transient is started (t < 30 s) is observed to be larger for cases with a higher heat flux despite having the same mass flux, pressure, and wall temperature values. This is attributed to mild improved heat transfer which is promoted by higher ratios of heat flux-to-mass flux. For heat flux-to-mass flux ratio values of $q_w"/G$ = 0.185 kJ/kg, improved heat transfer develops at the end of the pressure transient, as was observed in Figure 6. For higher values of $q_w"/G$, the wall temperature increases to a much higher value, and the Nusselt number is reduced at the end of the pressure transient which indicates deteriorated heat transfer. This agrees well with results in the published literature, where it is observed that improved heat transfer gives way to deteriorated heat transfer once $q_w"/G$ reaches sufficiently high values [1]. The Nusselt number in the deteriorated heat transfer region is slightly higher than the value of 160 predicted by the Dittus-Boelter correlation for an annular flow. This is due to the effect of the wire-wrap spacer on turbulent mixing, which was discussed previously. The Nusselt number at the end of the pressure-transient test case with $q_w"/G$ = 0.220 kJ/kg is considerably lower than the Nusselt number observed during deteriorated heat transfer at the end of the quasi-steady-state case in Figure 5, despite having similar values of $q_w"/G$. The fluid pressure in the quasi-steady-state test is $P/P_c$ = 1.07 which is farther from the critical pressure than the pressure of about $P/P_c$ = 1.02 at the end of the pressure transient tests of Figure 7 when deteriorated heat transfer is observed. This implies that greater deterioration in heat transfer occurs at the end of the pressure transient due to wall-normal property gradients that are significantly higher than those present in the quasi-steady-state test.

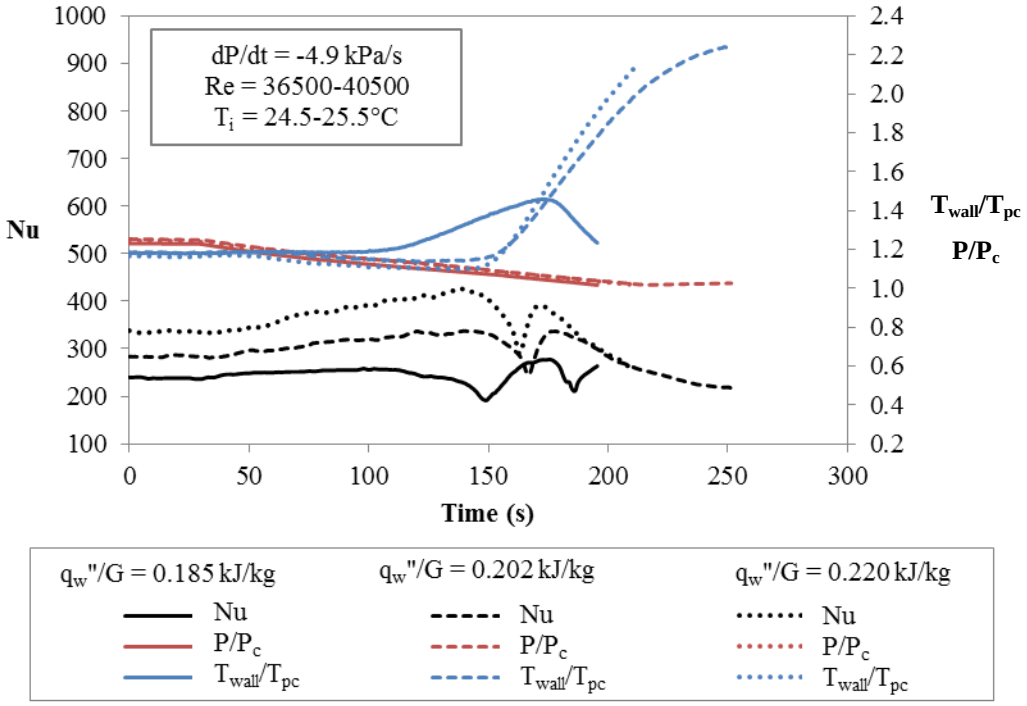


Figure 7 Effect of heat flux on the heat transfer process during pressure transients

Figure 8 presents the influence of varying the inlet temperature on heat transfer during pressure transients. Comparison of the trends in Figure 7 and Figure 8 suggests that raising the

inlet temperature of the test section causes deteriorated heat transfer to occur at a lower heat flux. In Figure 7, for Ti ~ 25°C, deteriorated heat transfer occurs when the heat flux-to-mass flux ratio exceeds about $q_w"/G$ = 0.2 kJ/kg, whereas deteriorated heat transfer occurs at $q_w"/G$ = 0.167 kJ/kg for Ti = 38°C in Figure 8, and at $q_w"/G$ = 0.156 kJ/kg for Ti = 47°C. For the same heat flux, raising the inlet temperature increases the bulk temperature at the measurement location. Therefore, the average temperature of the fluid near the wall moves closer to the pseudocritical temperature; this increases the magnitude of the wall-normal gradients of density and viscosity enabling the development of deteriorated heat transfer at lower values of wall heat flux.

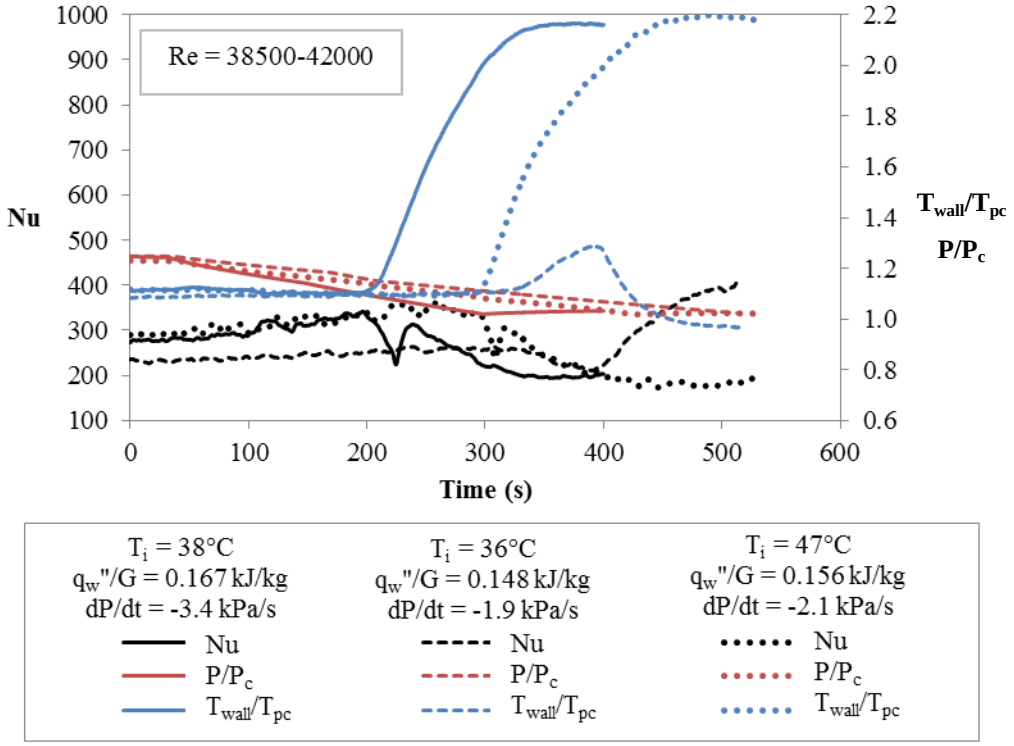


Figure 8 Heat transfer during pressure transients for a range of inlet temperatures

Several of the pressure transient cases were repeated at a Reynolds number of ~60000 to determine the dependency of the results on the Reynolds number. It was observed that at similar pressure transient rates, the temporal variation of the wall temperature was similar and the development of improved and deteriorated heat transfer at different heat flux-to-mass flux ratios and inlet temperatures was repeatable regardless of the value of the Reynolds number.

## 4. Conclusions

During heat transfer measurements at supercritical conditions in steady-state and transient tests, improved heat transfer and deteriorated heat transfer conditions are observed due to the changes in turbulent mixing promoted by wall-normal thermophysical property gradients. Improved heat transfer is consistently observed at lower heat-flux values whenever the wall temperature is near the pseudocritical temperature. As the heat flux is increased, improved

heat transfer transitions to deteriorated heat transfer; the reduction in the Nusselt number as heat transfer deteriorates increases considerably for pressures which are close to the critical pressure. During all instances of deteriorated heat transfer observed, the Nusselt number does not drop below the value predicted by the Dittus-Boelter correlation. This is deemed to be due to the enhanced turbulent mixing promoted by the wire-wrap spacer. The improvement in heat transfer due to the wire-wrap spacer is greater for flows near the thermodynamic critical point compared to flows at subcritical temperatures. Finally, it is noted that heat transfer during the pressure transients is not affected by the rate of the transience, which implies that the heat-transfer process is affected primarily by the local instantaneous state of the fluid.

## 5. References

[1] I. L. Pioro, H. F. Khartabil, and R. B. Duffey, "Heat transfer to supercritical fluids flowing in channels-empirical correlations (survey)", *Nuclear Engineering and Design*, Vol. 230, No. 1, 2004, pp. 69-91.

[2] H.S. Swenson, J. R. Carver, and C. R. Karakala, "Heat transfer to supercritical water in smooth-bore tubes", *Journal of Heat Transfer*, Vol. 87, No. 4, 1965, pp. 477-483.

[3] J. Licht, M. Anderson, and M. Corradini, "Heat transfer to water at supercritical pressures in a circular and square annular flow geometry", *Int. Journal of Heat and Fluid Flow*, Vol. 29, No. 1, 2008, pp. 156-166.

[4] H. Li, H. Wang, Y. Luo, H. Gu, X. Shi, T. Chen, E. Laurien, and Y. Zhu, "Experimental investigation on heat transfer from a heated rod with a helically wrapped wire inside a square vertical channel to water at supercritical pressures", *Nuclear Engineering and Design*, Vol. 239, No. 10, 2009, pp. 2004-2012.

[5] H. Wang, Q. Bi, Z. Yang, W. Gang, and R. Hu, "Experimental and numerical study on the enhanced effect of spiral spacer to heat transfer of supercritical pressure water in vertical annular channels", *Applied Thermal Engineering*, Vol. 48, No. 1, 2012, pp. 436-445.

[6] K. Kang and S. Chang, "Experimental study on the heat transfer characteristics during the pressure transients under supercritical pressures", *Int. Journal of Heat and Mass Transfer*, Vol. 52, No. 21, 2009, pp. 4946-4955.

[7] Kedare, S., Reinink, S., Hovell., K, Copping, A., and Yaras, M. I., "Carleton R134a thermalhydraulics loop: wire-wrap spacer pitch based on annular flow heat transfer and pressure loss experiments", Technical Report CU-M&A-2013-04, 2013.

[8] C. Azih and M. I. Yaras, "Direct numerical simulations of laminar and turbulent forced-convection heat transfer in channels with supercritical water", The 6th Int. Symposium on Supercritical Water-Cooled Reactors, Shenzhen, China, 2013.

[9] C. Azih, J. R. Brinkerhoff, and M. I. Yaras, "Direct numerical simulation of convective heat transfer in a zero-pressure-gradient boundary layer with supercritical water", *Journal of Thermal Science*, Vol. 21, No. 1, 2012, pg 49-59.